https://doi.org/10.5194/egusphere-2025-5495
Preprint. Discussion started: 24 November 2025

Unexpected quasi-independence of colored dissolved organic matter absorption from chlorophyll-a concentration in the Southern Ocean

Juan Li[1,2*], David Antoine[1,2], and Yannick Huot[3]

[1] Remote Sensing and Satellite Research Group, School of Earth and Planetary Sciences, Curtin University, Bentley, WA 6102, Australia
[2] ARC Australian Centre for Excellence in Antarctic Science (ACEAS), University of Tasmania, Hobart, TAS 7001, Australia
[3] Centre d'Applications et de Recherches en Télédétection, Département de géomatique appliquée, Université de Sherbrooke, Sherbrooke, Québec J1K 2R1, Canada
* Now at : International Research Laboratory Takuvik, CNRS – Université Laval – Sorbonne Université, avenue de la Médecine, Département de Biologie, Université Laval, Québec, QC G1V0A6, Canada

Correspondence to: Juan Li (juan.li@takuvik.ulaval.ca)

Abstract. The absorption coefficient of colored dissolved organic matter (CDOM), a_y, plays a critical role in driving ocean optical properties and so light attenuation and light-dependent biogeochemical cycles. In the Southern Ocean (SO), however, a_y remains poorly documented because of the scarcity of in situ measurements and the absence of suitable bio-optical models. To address this gap, we derived a_y in surface waters from the diffuse attenuation coefficient (K_d) derived from radiometric measurements performed by Biogeochemical-Argo floats. Sensitivity analyses indicated that the uncertainty of our estimates is mainly driven by K_d, with an overall ~18% uncertainty of a_y at 380 and 412 nm based on a Monte Carlo approach. The relationships we obtained between a_y and Chl in low-latitude waters are consistent with previous studies but diverge in the SO, with a much weaker dependence on Chl and a larger relative contribution to the absorption budget for clear waters. Possible reasons for this different contribution include CDOM release by sea ice melting, CDOM enrichment of surface layers through deep winter mixing, adaptation of phytoplankton physiology to cold waters and reduced photo degradation during the polar winter.

1 Introduction

Colored dissolved organic matter (CDOM) is the fraction of the dissolved organic matter (DOM) pool that absorbs light in the ultraviolet and visible region of the spectrum. This absorption reduces light penetration into the water column, thereby influencing phytoplankton dynamics, nutrient cycling, primary productivity, and the overall biological carbon pump (Nelson and Siegel, 2002; Siegel et al., 2002; Nelson and Siegel, 2013; Mannino et al., 2014). Therefore, CDOM plays a crucial role in the biogeochemical cycles and optical properties of the world's oceans, including the Southern Ocean (SO), a key component of the global carbon cycle (Gruber et al., 2009, 2019; Hauck et al., 2023; Boyd et al., 2024). It is accordingly important to quantify the CDOM distribution for better understanding of the biogeochemical processes underlying its variability. In addition, the high CDOM absorption in the blue part of the spectrum adds to phytoplankton absorption in that spectral range, which means that accurately quantifying CDOM absorption is also of paramount importance to a proper derivation of the phytoplankton chlorophyll-a concentration (Chl, mg m^{-3}) from satellite ocean color measurements.

While the number of CDOM absorption measurements are increasing in global databases, as for any dynamic variable, in situ observation will always under-sample the ocean. This is even more true in the SO where logistical difficulty and the harsh environment mean that we have extremely limited in situ studies of CDOM. In response, a number of studies have emerged to inverse the absorption of CDOM (a_y, m^{-1}) using ocean color remote sensing (OCRS) but mostly for non-polar waters. These approaches include empirical algorithms such as band-ratios algorithms (Mannino et al., 2008; Morel and Gentili, 2009; Mannino et al., 2014; Cao et al., 2018), fitting of a_y with the diffuse attenuation coefficient (Mannino et al., 2014), and multiple linear regression between a_y and remote-sensing reflectance (Aurin et al., 2018). Other methods encompass inherent optical properties (IOPs)-based semi-analytical algorithms (Carder et al., 1999; Matsuoka et al., 2013; Loisel et al., 2014; Mannino et al., 2014; Chen et al., 2017; Bonelli et al., 2021), quasi-analytical algorithms (Lee et al., 2002; Zhu et al., 2011; Zhu and Yu, 2013), and purely statistical techniques such as the principal component analysis (PCA) algorithm (Cao and Miller, 2015) and end-member analysis algorithm (Houskeeper et al., 2021).

However, the bio-optical properties of the SO are statistically different from low-latitude waters, which has been recently shown in its distinctive bio-optical properties of phytoplankton (Robinson et al., 2021) and the high proportion of non-algae particles (NAP) in oligotrophic waters (Li et al., 2024). This implies that empirical algorithms developed for other oceans to interpret ocean color observations in the SO will likely be biased. As an example, because CDOM and NAP have similar spectral shapes that are difficult to distinguish in the reflectance measurement, many ocean color algorithms retrieve the absorption of colored detrital matter a_{CDM} (m^{-1}) which represents their sum. These can be subsequently separated in post processing by using empirical relationships. For instance, the contribution of NAP is often approximated as a function of the particulate backscattering coefficient (b_{bp}, m^{-1}) (Zhu et al., 2011; Matsuoka et al., 2013). Whether a_{NAP} is correlated with b_{bp} remains unknown for the SO, however, due to a lack of in situ data. Furthermore, purely statistical approaches lack a firm analytical and theoretical basis, making their results difficult to interpret (Zhu et al., 2014). Overall, none of the existing algorithms has been specifically developed or thoroughly validated for the SO, highlighting the need for a robust inversion algorithm tailored to this region to quantify CDOM distribution and then to improve our understanding of its role in biogeochemical cycles and response to climate change.

Thanks to the deployments of autonomous profiling Biogeochemical-Argo (hereafter BGC-Argo) floats in the SO by, e.g., the Southern Ocean Carbon and Climate observations and Modeling (SOCCOM; Sarmiento et al., 2023) or the Remotely-sensed Biogeochemical Cycles in the Ocean (RemOcean; Claustre et al., 2020) programs, the availability of in situ data has increased, making them the only in situ platform capable of investigating the properties of a_y at large spatial scales. When integrated with ship-based measurements from Antarctic research expeditions, these float data can contribute tremendously to the understanding of a_y-related bio-optical properties of the SO. In this study, we used a simple semi-analytical approach to estimate a_y from float measurements. Uncertainties were quantified through sensitivity analyses and Monte Carlo simulations. We then compared a_y-related bio-optical properties and relationships between the SO and low-latitude waters to explore potential mechanisms underlying their differing distributions.

2 Data and methods

2.1 Data selection from BGC-Argo floats

We used a total of 60 BGC-Argo floats deployed in the SO (south of 40° S in this study) between 29/11/2013 and 02/05/2025, and 211 floats deployed in low-latitude regions (from 40° S to 60° N) from 22/10/2012 to 26/12/2024. These floats are equipped with Seabird CTD sensors for temperature and salinity, Seabird/Satlantic OCR-500 multispectral radiometers collecting downward plane irradiance (E_d, μW cm^{-2} nm^{-1}) at 380, 412 and 490 nm, and Seabird/WET Labs ECO-series sensors providing the total optical backscattering coefficient at 700 nm ($b_b(700)$, m^{-1}) and chlorophyll fluorescence. Overall, these floats had collected 10,579

(SO) and 38,615 (low latitudes) profiles during the period indicated.

For each of the floats, we first eliminated profiles collected in shallow waters (depth < 200 m) based on the global relief ETOPO1 data base (NOAA, 2009), as well as profiles for which the Sun elevation was < 15° at the end of the upcast. Then, for chlorophyll, backscattering and radiometry we only kept profiles flagged "A" (100% of good data) or "B" (at least 75% of good data), as per the nomenclature of the Argo data management team (Argo data management, 2025). For the profiles passing this first screening, only data points with a quality flag set to either 1 (good), 2 (probably good), 5 (value changed) or 8 (interpolated value) were kept. The total of data points flagged either 1 or 2 was from 80% to 98% of the entire data set depending on the parameter.

The locations of profiles that passed these quality controls (roughly one third of the total) are displayed in Fig. 1, and the number of profiles eliminated after each step of quality control are summarized in Table S1. The temporal coverage of the selected profiles across years and months is displayed in Fig. S1. The distribution of the sun zenith angles is depicted in Fig. S2a, while Fig. S2b shows the irradiance just above the surface for λ = 490 nm, limited to cases within 20% of the theoretical clear-sky value calculated following Gregg and Carder (1990).

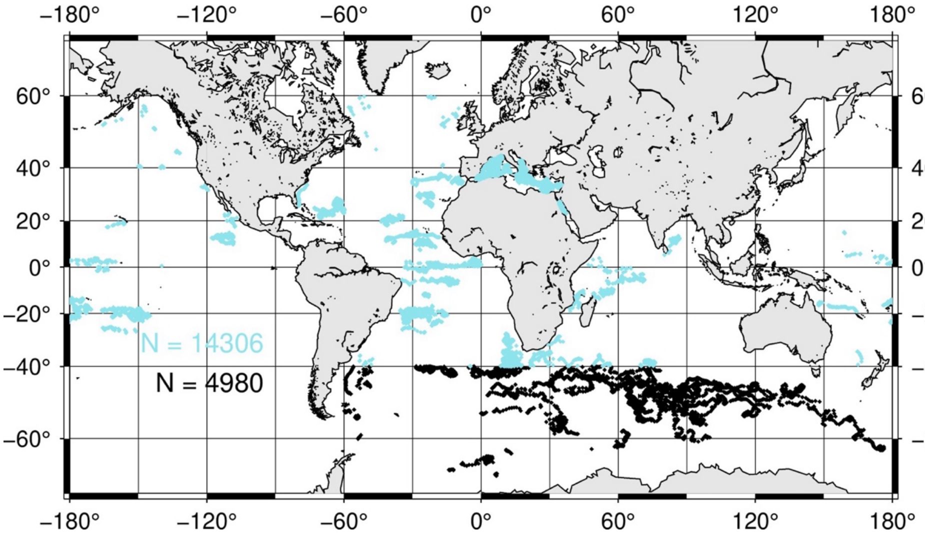

Figure 1: Surface locations of the BGC-Argo float profiles used in this study for the SO (black) and elsewhere (blue), after various screenings have been applied to the full data set (see methods).

2.2 From radiometric measurements to K_d

The overall workflow we used to then process the BGC-Argo data is displayed in Fig. S3. We did not correct the radiometry data for dark deep values, which have been shown to be negligible (Organelli et al., 2016). We checked these values and indeed they were always lower than 10^{-3} mW cm^{-2} nm^{-1}, with a distribution centered on 10^{-4} mW cm^{-2} nm^{-1}.

Then a 4th order polynomial was fitted to the data to clean the $E_d(z,\lambda)$ profiles from changes due to possible changes in the above-water downward irradiance caused by clouds and from near surface fluctuations generated by waves. This fit was only performed if more than 20 valid data points were available, otherwise the profile was eliminated. This fitting procedure is similar to what Organelli et al., (2016) did, although we did not find it necessary to repeat the 4th order polynomial in order to get smooth profiles. The K_ds were then calculated in three different ways from the fitted E_d profile, to allow a sensitivity study about the K_d value. The first one (K_d(0-20 m)) was calculated from E_d(z=0$^-$) and E_d(z=20 m). This way mimics the methodology used in most of the field data sets by Morel (1988) and later revised by Morel and Maritorena (2001) (hereafter MM01), and it is taken here as the reference

https://doi.org/10.5194/egusphere-2025-5495
Preprint. Discussion started: 24 November 2025

for the low-latitude environments. At that time, profiling radiometers were not yet available; instead, radiometers were deployed using winches and stabilized at successive depths where measurements were collected. A depth of about 20 m was typically chosen, as irradiance fluctuations were sufficiently dampened to ensure reliable E_d measurements. The second K_d calculation ($K_d(Z_{\rm pd})$ was similar but used E_d at the first optical depth ($Z_{\rm pd}$) rather than at 20 m. This depth was calculated for each wavelength and corresponds to the point where E_d is reduced to 1/e of its below-surface value. At this stage, we added another quality control by eliminating profiles when $Z_{\rm pd}$ deviated by more than a factor of 2.5 (either greater or lower) from the value predicted from Chl using MM01. The third calculation took the mode of the distribution of local K_d values, computed at each measurement depth within successive 5 m intervals from just below the surface down to the first optical depth. K_d(0-20 m) is the one used in subsequent analyses.

2.3 Chlorophyll and backscattering from BGC-Argo floats

The Chl values delivered by the BGC-Argo program are derived from chlorophyll fluorescence scaled to Chl using manufacturers calibration parameters and further divided by a factor of 2 following recommendation by Roesler et al., (2017). A similar correction was recommended for SO phytoplankton by Roesler et al., (2017), however, with a factor of 3.79 instead of 2. Therefore, the SO Chl data were multiplied by a factor of 2/3.79. Each Chl and total backscattering profiles were adjusted by shifting the whole profile so that the average value between 200 and 400 dbars equals the mode of the distribution of deep values calculated over the same depth range from all profiles of all floats. This adjustment was performed to account for the potential bias between different measurement technologies and for possible instrument drift. These deep values were 0.0055 mg Chl m^{-3} and 3×10^{-4} m^{-1}. After this procedure, we found 2070 values of surface Chl lower than 0.02 mg m^{-3} (15% of the data). This is unrealistic, as the minimum concentrations ever measured in the upper layers of the ocean are about 0.02 mg m^{-3}, e.g., in the southeast Pacific gyre (Morel et al., 2007b). The use of a single factor of 2 for the fluorescence to Chl conversion is likely responsible for such underestimations, which is consistent with the high variability actually reported for this factor by Roesler et al., (2017). Instead of artificially truncating the data set at Chl values < 0.02 mg m^{-3}, we re-adjusted the deep values to an average of 0.02 mg m^{-3}. This admittedly subjective adjustment allowed avoiding unrealistic low Chl values while keeping consistency in the deep adjustment. The impact on any Chl > ~0.1 mg m^{-3} goes from about 15% to negligible.

Similarly to what was done for the radiometry profiles, a 4th order polynomial was fitted to the inherently noisy Chl and backscattering profiles using data from the top 50 m only. Finally, average surface Chl, $b_{bp}(700)$, temperature (T, °C) and salinity (S, psu) were calculated over the first optical depth for $\lambda = 380$ nm determined from the radiometry profiles. The average T and S were subsequently used to calculate the seawater backscattering coefficient (b_{bw}, m^{-1}) according to Zhang and Hu (2009) and Zhang et al., (2009), which is subtracted from the total backscattering coefficient to get the particulate backscattering coefficient, b_{bp}. The resulting distributions for Chl and b_{bp} are illustrated in Fig. S2c,d. The contribution of seawater to the diffuse attenuation coefficient for downward irradiance, K_w, is approximated as $a_w + b_{bw}$, where a_w is the absorption of seawater and its value can be found in Lee et al., (2015).

2.4 Ship-based measurements

The particulate and CDOM absorptions, a_p (m^{-1}) and a_y (m^{-1}), form the bulk of the total non-water absorption. Therefore, to determine a_y we need as realistic as possible estimates of a_p. For the low-latitude oceans, we used the a_p vs. Chl relationships from Bricaud et al., (1998). For the SO, we used ship-based field data acquired during two Southern Ocean research voyages: the

Antarctic Circumpolar Expedition (ACE) aboard the RV Akademik Tryoshnikov during the Austral Summer from 20 December 2016 to 19 March 2017 (Robinson et al., 2021), and the Southern Ocean Large Areal Carbon Export (SOLACE) research voyage aboard the RV Investigator (voyage IN2020_V08) from 05 December 2020 to 16 January 2021.

Water samples were collected during the ACE and SOLACE either 3-hourly from the underway seawater supply (sampling depth ~5 m) or from the shallowest depth of the CTD (conductivity, temperature, and depth) rosette casts. Phytoplankton pigment concentrations were determined using high performance liquid chromatography (HPLC, see details in Ras et al. 2008 and references therein). Total Chl was defined as the sum of mono- and divinyl chlorophyll a concentration, chlorophyllide a, and the allomeric and epimeric forms of chlorophyll a (Hooker and Zibordi, 2005; Reynolds et al., 2016). Particulate absorption (a_p) measurements were made on the same filters analyzed for pigments. A full description of the measurement protocols and the data are available in Antoine et al., (2021) and Robinson et al., (2021). The resulting a_p vs. Chl relationships are displayed in Fig. S4.

Measurements of ay are unfortunately seldom carried out at sea, leaving us with few options for validating the ay estimates. We did not have any such data for the SO. For the low-latitude areas, we used three data sets of field a_y measurements. The first one is from the Bouée pour l'acquisition d'une Series Optique à Long terme (BOUSSOLE) in the Mediterranean Sea (Antoine et al., 2006). Measurements were carried out at this site from 2011 to 2015, and the initial years of data have been presented by Organelli et al., (2014). The second data set is from the BIogeochemistry and Optics SOuth Pacific Experiment (BIOSOPE) that occurred in 2004 in the Southeast Pacific Ocean (Claustre et al., 2008), with the ay data analyzed by Bricaud et al., (2010). The third data set (18 data points out of the SO) was extracted from the NASA Nomad data base (Werdell and Bailey, 2005). The Mediterranean Sea is known to display higher-than-average CDOM absorption per Chl, while the Southeast Pacific Ocean exhibits the opposite pattern . Therefore, the BOUSSOLE data set is expected to match the upper part of the distribution of the ay values derived here when plotted as a function of Chl, while the BIOSOPE data would rather match the lower part of that distribution.

2.5 a_y inversion model

The $K_d(\lambda)$ can be expressed as a function of IOPs as follows (Gordon, 1989; Morel et al., 2007b):

$$K_d(\lambda) = 1.0395\,\frac{a(\lambda)+b_b(\lambda)}{\mu_d(\lambda)}, \tag{1}$$

where μ_d is the average cosine of $E_d(0^-,\lambda)$, $a(\lambda)$ and $b_b(\lambda)$ are the total absorption and backscattering coefficients, which can be expanded as follows:

$$a(\lambda) = a_w(\lambda) + a_p(\lambda) + a_y(\lambda), \text{ and} \tag{2}$$

$$b_b(\lambda) = b_{bw}(\lambda) + b_{bp}(\lambda). \tag{3}$$

The contribution of CDOM to scattering is neglected in this study (Dall'Olmo et al., 2009). When substituting Eq. (2)~(3) into (1), $a_y(\lambda)$ can be solved as:

$$a_y(\lambda) = \frac{K_d(\lambda)\mu_d(\lambda)}{1.0395} - a_w(\lambda) - a_p(\lambda) - b_{bw}(\lambda) - b_{bp}(\lambda), \tag{4}$$

where $a_w(\lambda)$ is assumed constant (values from Lee et al., 2015) and $b_{bw}(\lambda)$ is calculated using measured temperature and salinity by BGC-Argo floats following Zhang and Hu (2009) and Zhang et al., (2009). Particulate absorption can be described as a function of Chl based on in situ relationships. For the SO, to account for the high contribution of NAP in oligotrophic waters (Li et al., 2024), a background constant was added to the power-law regression between $a_p(\lambda)$ and Chl:

$$a_p(\lambda) = \mathrm{const}(\lambda) + \chi(\lambda)\mathrm{Chl}^{e(\lambda)}, \tag{5}$$

where the exponent $e(\lambda)$ and the factor $\chi(\lambda)$ are derived from concurrent measurements of Chl and $a_p(\lambda)$ is the SO (see Fig. S4) or from Bricaud et al., (1998) for the low-latitude waters. Note that the tabulated data from Bricaud et al., (1998) do not include wavelengths < 400 nm, however, so we estimated values at 380 nm by extrapolating from their Fig. 4.

$b_{bp}(\lambda)$ is converted from $b_{bp}(700)$ following

$$b_{bp}(\lambda) = b_{bp}(700)\left(\frac{700}{\lambda}\right)^{\eta}, \tag{6}$$

where η equals to 1.08 for the SO, which is the mean value based on data collected during the ACE and SOLACE cruises (Li et al., 2024). While for the low-latitude waters, a value of 1.03 is adopted to be consistent with the value used in the GSM01 model developed by Maritorena et al., (2002) for non-polar waters. Chl and $K_d(\lambda)$ are obtained from the floats' measurements (see above). The average cosine, μ_d, which is a function of Chl, λ and sun zenith angle (θ_s, equals to 90 minus sun elevation) under clear or overcast sky conditions, was derived using the lookup tables (LUT) developed by Morel et al., (2002) and Morel and Gentili (2004). To determine whether a profile is collected under clear or overcast sky conditions, the spectral solar irradiance model of Gregg and Carder (1990) was implemented to generate the downward irradiance at 490 nm just below the ocean surface. If the absolute difference between the calculated and measured $E_d(0^{-}$,490) is within 20%, then the sky is assumed clear, otherwise it was classified as overcast.

2.6 Sensitivity studies

2.6.1 Individual parameters

The many steps of quality control performed on the E_d profiles might not fully eliminate bad data from unsupervised BGC-Argo measurements. The impact on deriving K_d must be assessed, as it is the first uncertainty when deriving ay using Eq. (4). The three K_d estimates presented above were derived for this purpose.

The average cosine of the downward irradiance, md, is a second source of uncertainty when using Eq. (4). The μ_d is taken from the LUTs that have been generated through a bio-optical model, which cannot be always appropriate for any bio-optical conditions (e.g., Morel et al., 2007a). The sensitivity study was conducted by either using the clear vs. cloudy sky test (Fig. S2), in which case md was taken from the corresponding LUT (referred to as md actual), or by using only the md for clear sky or only the md for overcast conditions. In doing this, we assumed that the difference in md between the clear-sky (md between 0.68 and 0.92) and the overcast conditions (μ_d=0.8) is of the same order of magnitude than the difference caused by variability in bio-optical properties.

The third significant source of uncertainty comes from a_p. This coefficient was derived from its average relationship to Chl, which cannot account for local departure from these relationships. Three relationships were used to assess the impact on ay (Fig. S4): our SO relationship with (referred to SO dataset (Eq.5)) and without (SO dataset) a constant background value, and the one from Bricaud et al., (1998).

No individual sensitivity study was performed on b_{bw} and b_{bp} because of their small contribution in Eq. (4) and the rather well-constrained values for b_{bw}. The aw value only represents a large contribution to the total absorption in clear waters at 490 nm. Therefore, it was neither individually assessed here.

2.6.2 Monte Carlo approach

The sensitivity studies to individual parameters cannot provide an overall uncertainty for a_y as derived through Eq. (4). Therefore, we also conducted a systematic assessment of uncertainty using a Monte Carlo method. This approach involved running Eq. (4) 10,000 times for a given set of inputs, by introducing random uncertainties to each input in each run. For a given parameter, the random uncertainties were generated by multiplying an average absolute or relative uncertainty by a random number within the [–

0.5, +0.5] range. The absolute or relative type B uncertainties are provided in Table 1. The repeated calculations generated a set of 10,000 a_y values for each K_d value, and the standard deviation of their distribution was used as a measure of uncertainty in a_y. The advantage of such an approach is that an uncertainty can be derived for each individual a_y value. This approach does not address potential significant biases in the K_d values.

Table 1 Individual uncertainties used in the Monte Carlo method

		wavelength			
Parameter		380 nm	412 nm	490 nm	Comments
K_d	R✦	30%			Jamet et al., (2012)
μ_d	A	0.1			Twice the standard deviation of md values calculated for all profiles
Chl	R	35%			Moore et al., (2009)
Const(l)*	A	0.00063	0.00056	0.00038	
c(l)*	A	0.0018	0.0016	0.0010	From the nonlinear regressions in Fig. S4
e(l)*	A	0.075	0.057	0.046	
b_{bp}	R	20%			Standard deviation in deep values
a_w	A	0.0008 m^{-1}	0.0005 m^{-1}	0.0005 m^{-1}	Lee et al., (2015)
b_{bw}	A	0	0	0	Considered negligible (changes are < 1×10^{-5} m^{-1} for changes in T and S of 5 degrees or 5 psu, for instance)

✦ R or A in this column indicate either a relative or absolute error.

* See Eq. (5) for a_p vs. Chl.

3 Results

3.1 Overall performance of the a_y derivation from K_d

The relative contributions of the various terms in Eq. (4) were derived from the entire data set (Fig. 2). They determine the sensitivity of the derived a_y to these parameters and are analysed here to support the results of the sensitivity analyses shown in Fig. 3. At 380 nm, apart from the highest Chl concentration, a_y contributes to more than 40% of the total absorption plus backscattering budget, and up to near 60% for Chl around 0.2 mg m^{-3} for low-latitude waters and for Chl around 0.05~0.1 mg m^{-3} for the SO. These percentages create favorable conditions to operate Eq. (4). As expected from the spectral dependence of a_y, the situation is less favorable for longer wavelengths, with percentages ranging from about 30% to 50% at 412 nm and from about 20% to 30% at 490 nm (see Fig. S5). Fig. 2 also shows that the relative contribution of a_y to the absorption budget is larger for clear waters of the SO than for clear waters of the low-latitude oceans.

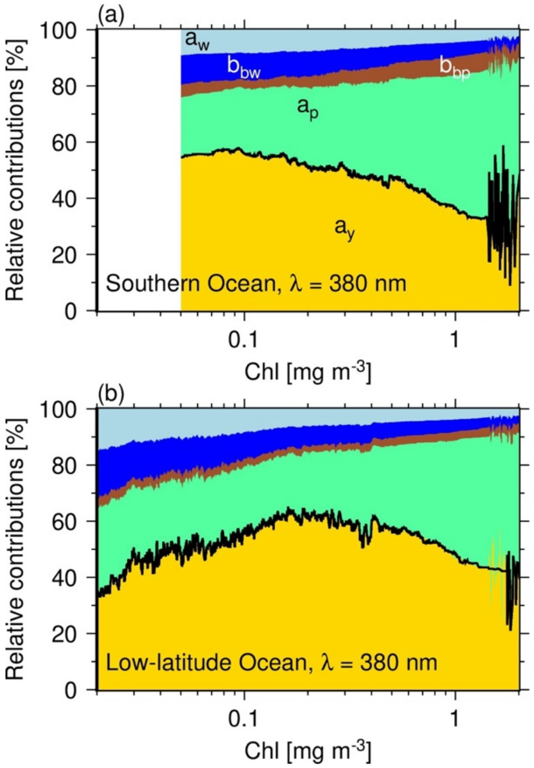

Figure 2: Relative contributions of a_w (light blue), b_{bw} (blue), b_{bp} (brown), a_p (green) and a_y (gold) in Eq. (4) at λ = 380 nm, as a function of Chl. Panel (a) is for the SO and (b) is for the low-latitude Oceans. The thick black line delineates the contribution of $a_y(380)$ to this budget. The increased noise in that curve for Chl > ~1.3 mg m^{-3} arises from the limited numbers of retrievals in this range.

At 380 nm in the SO, there is little sensitivity of the overall distribution of the derived a_y to different approaches to obtain K_d (Fig. 3a), μ_d (Fig. 3b) and a_p (Fig. 3c). As expected, K_d is the main contributor to the differences in a_y, followed by a_p and μ_d. Results are similar at the 412 and 490 nm and for the low-latitude waters (Table 2), except for a_p at 412 nm in low-latitude oceans. They show increasing sensitivity to the three parameters with increasing wavelength.

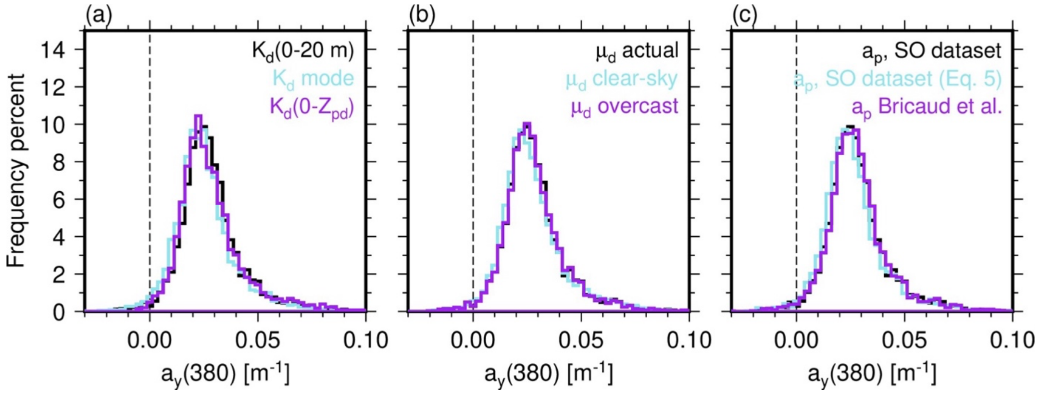

Figure 3: Distribution of $a_y(380)$ resulting from (a) three approaches to obtain K_d from $E_d(z, 380)$, (b) whether the distinction between clear and cloudy sky is applied or ignored when calculating μ_d, and (c) using the three different a_p vs. Chl relationships displayed in Fig. S4. Data for the SO only.

https://doi.org/10.5194/egusphere-2025-5495
Preprint. Discussion started: 24 November 2025

Table 2 Average dispersion (%) of the mean a_y values with respect to their average for the three instances of each sensitivity study and the three wavelengths

	380 nm	412 nm	490 nm
SO			
K_d	6.8	11.4	30.9
μ_d	1.5	1.1	1.1
a_p	4.4	9.6	31.7
Low-latitude oceans			
K_d	6.4	13.5	45.0
μ_d	1.1	1.3	3.7
a_p	7.0	0.8	21.4

The results of the Monte Carlo analysis applied to the SO data set are displayed in Fig. 4, as the distribution of the coefficient of variation (CV, defined as 100 × standard deviation divided by the mean) of $a_y(\lambda)$ values obtained for each individual estimate of $K_d(\lambda)$. Each CV results from 10,000 runs of Eq. (4) using randomly picked errors on the individual terms of the equation (see methods). The modes of the histograms show that an uncertainty around 18% can be generally expected for λ = 380 and 412 nm, and 25% for λ = 490 nm. Cumulative curves (not shown) indicate that 85% of uncertainties are lower than 20% for λ = 380 nm, 60% at 412 nm and 20% at 490 nm, reemphasizing that the band at 490 nm is far less adapted to deriving a_y from Eq. (4) than the two other bands.

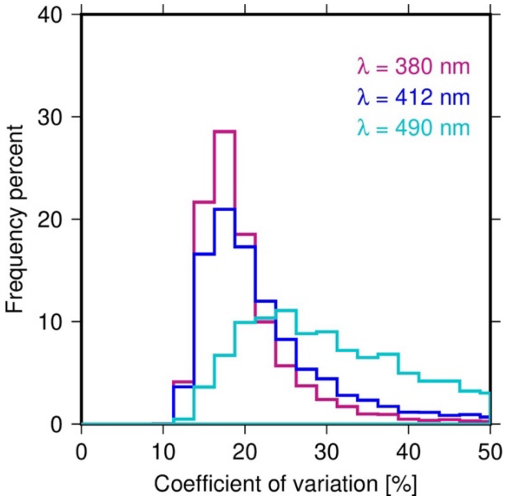

Figure 4: Distribution of the coefficient of variation of $a_y(\lambda)$ values obtained by running the Monte Carlo analysis on each of the individual estimates of $K_d(\lambda)$.

3.2 $K_{bio}(\lambda)$ vs. Chl relationships

Unbiased retrievals of $K_d(\lambda)$ are essential to our study. Therefore, we first assessed whether our retrievals were consistent with bio-optical relationships previously established for the low-latitude oceans under the form of the K_{bio} vs. Chl relationship, where K_{bio} is $K_d - K_w$, representing the contributions of all non-water components. The results of low-latitude oceans are displayed in

Figs. 5a,b,c, along with the MM01. The χ coefficients and the exponents of the K_{bio} vs. Chl relationships are within 15% of those from MM01 at 380 and 412 nm and differ by about 45% at 490 nm. The r^2 are accordingly decreasing from 0.5 at 380 nm to 0.33 at 490 nm. The slopes (exponents) of our relationships are lower than those from MM01. Despite these differences, these results show that the method used here can derive an overall consistent picture of the K_{bio} vs. Chl relationship for areas where it is well established. It is therefore providing the basis to apply it to the SO, where no such reference exists.

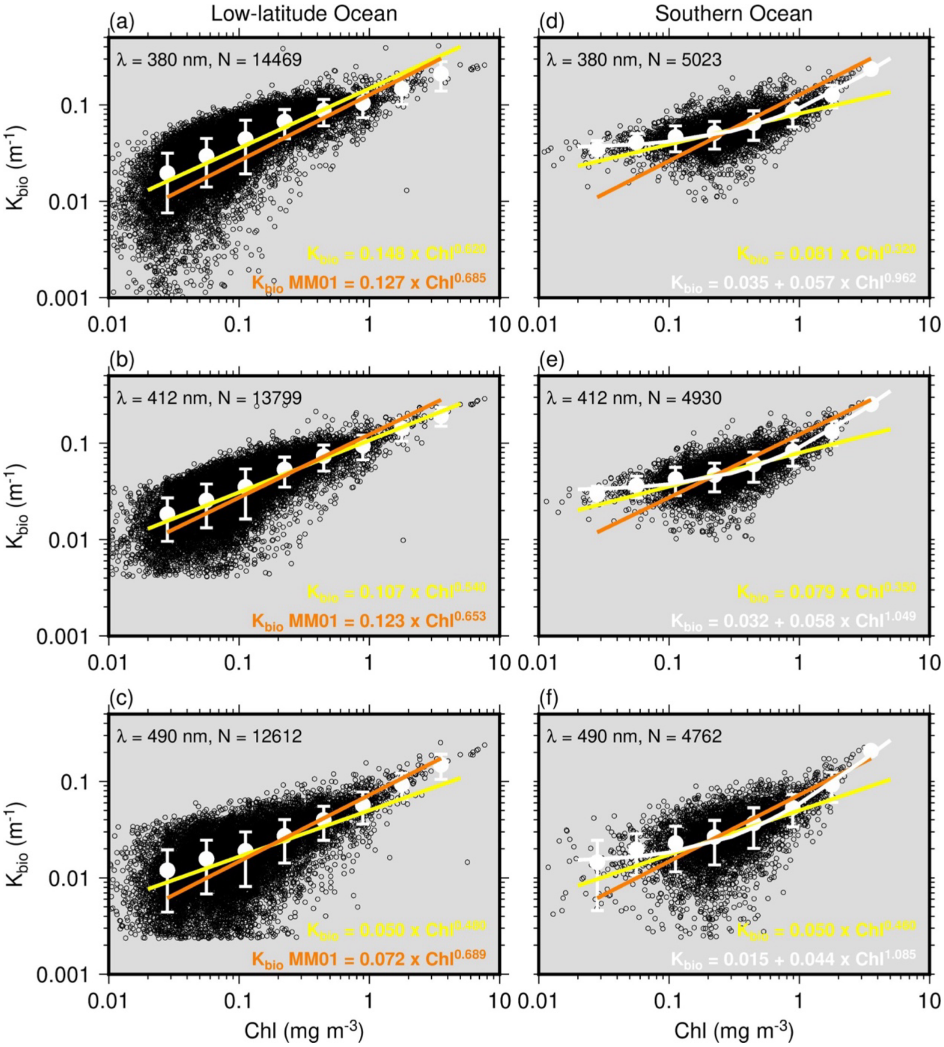

Figure 5: Non-water diffuse attenuation coefficient for downward irradiance (K_{bio}) for the three wavelengths indicated and for the low-latitude oceans (left) and the SO (right) data sets. The black dots are all data obtained from individual float profiles. The white circles and vertical bars are average values and their standard deviation calculated over logarithmically equal Chl intervals. The yellow and white solid lines are a linear and a non-linear fits to all data points (log-transformed data; equations reported on each panel), and the orange line and "K_{bio} MM01" equation are for the Morel and Maritorena (2001) model.

The results of the SO are displayed in Fig. 5d,e,f. Here the Chl range is smaller than in the low-latitude data set, spanning from about 0.05 mg m^{-3} (very few points below this value) to 3 mg m^{-3}. The $K_{bio}(\lambda)$ values have the largest variance in the medium Chl range (0.1~1 mg m^{-3}) in the SO. They do not follow the same decreasing trend as for the low-latitude oceans in the low Chl range (< 0.2 mg m^{-3}), which is likely partly driven by the larger $a_p(\lambda)$ values as compared to what is observed in low-latitude areas (e.g., Bricaud et al., 1998; Fig. S4). The MM01 relationships seem to fit our data quite well for Chl > ~0.5 mg m^{-3}. They do not match the data at lower Chl values, and the fit using a function of the form $K_{bio}(\lambda) = \chi\ \mathrm{Chl}^{e}$ as in MM01 also fails to capture this range. A better fit is obtained with a formulation similar to the one used for a_p (Eq. 5), as displayed as the white curves in Fig. 5d,e,f, showing a low dependence of K_d on Chl below Chl ~0.2 mg Chl m^{-3}.

3.3 $a_y(\lambda)$ vs. Chl relationships

Similarly to $K_{bio}(\lambda)$, we analyzed a_y as a function of Chl (Fig. 6). The relationships we obtained for the low-latitude areas are similar to those proposed by Morel and Gentili (2009) (hereafter MG09), except for λ = 490 nm, where the dispersion of the a_y values is the largest, as expected from the methodology. Therefore, results at this wavelength must be cautiously considered. Given the MG09 was originally developed at 400 nm and subsequently extended to other wavelengths using a spectral slope of 0.018 nm^{-1}, and our a_y at 412 nm is the closest match to 400 nm, therefore, here we compare it with MG09 at 412 nm to minimize the potential discrepancy that might occur from wavelength conversions involving larger spectral distance. In low-latitude waters, MG09 generally aligns with our predicted $a_y(412)$ vs. Chl relationship, apart from Chl > 3.0 m^{-3}, where additional data is required for further assessment. This further confirms the validity of our float-based inversion approach.

https://doi.org/10.5194/egusphere-2025-5495
Preprint. Discussion started: 24 November 2025

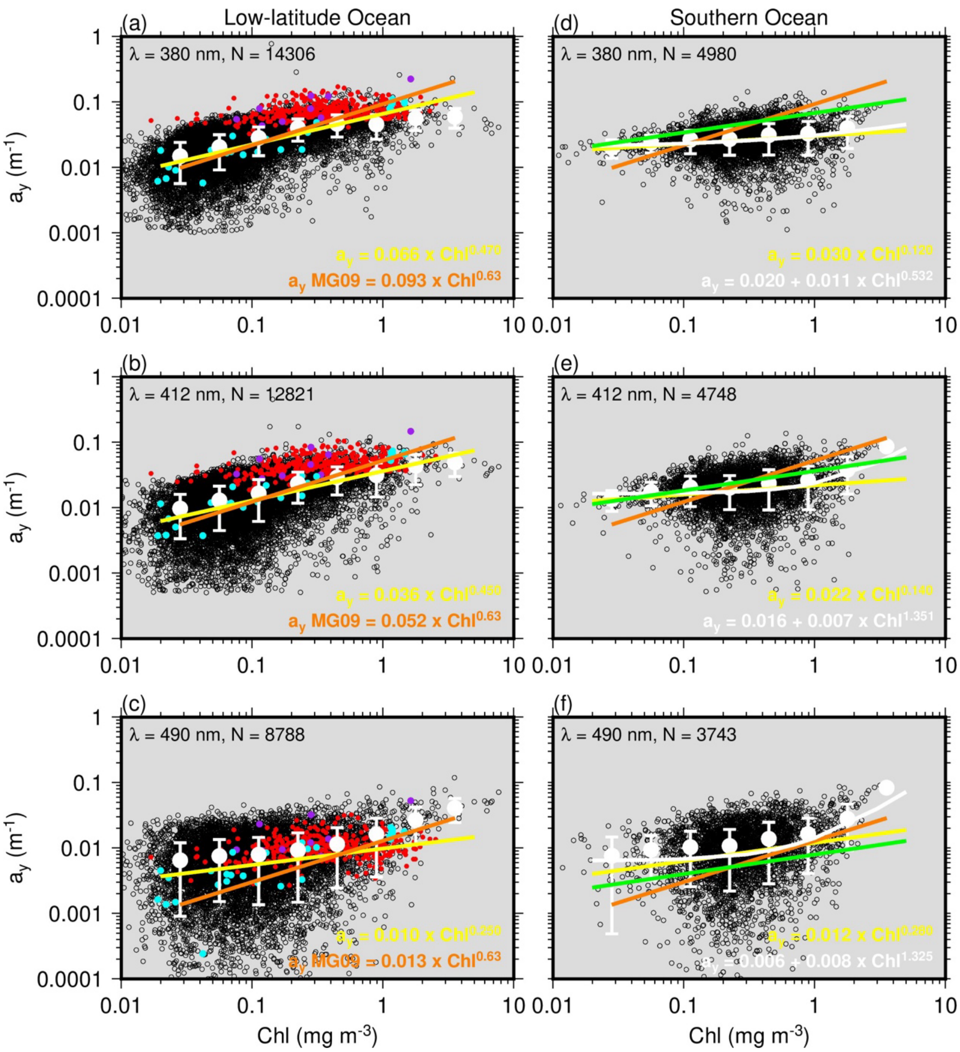

Figure 6: CDOM absorption (a_y) for the three wavelengths indicated and for the low-latitude waters (left) and the SO (right) data sets. The black dots are all data obtained from individual float profiles. The white circles and vertical bars are average values and their standard deviation calculated over logarithmically equal Chl intervals. The yellow and white curves are a linear and non-linear fits to all data points (log-transformed data), the orange lines are from the Morel and Gentili (2009) model, whose equations are also reported as "a_y MG09", and the green lines are from Reynolds et al., (2001). In panels (a), (b) and (c), the colored dots are *in situ* measurements of a_y from the BOUSSOLE site in the Mediterranean Sea (red dots), the BIOSPOPE research voyage in the Southeast Pacific gyre (turquoise), and the NOMAD data set (purple) that covers various oceans.

The BOUSSOLE data sit on the upper part of the data cloud and the BIOSOPE data rather in the middle of it, with some low values for low Chl, which is consistent with what has already been shown for the Mediterranean Sea and the Southeast pacific gyre (Morel et al., 2007b). The NOMAD data are also on the high range. This consistency of the derived a_y with field measurements further validates the approach.

In the SO (Fig. 6d,e,f), a_y does not vary much across the whole Chl range, with slopes of the a_y vs. Chl relationships much lower than those of the low-latitude data set and the MG09 model (equations reported on each panel of Fig. 6). The regression coefficient of the relationship at 380 nm in low-latitude waters is 0.26, whereas for the SO it is less than 0.1 across all wavelengths.

Reynolds et al., (2001) have reported an a_y vs. Chl relationship for the Ross Sea and Antarctic Polar Front Zone, expressed as $a_y(400) = 0.046\ \mathrm{Chl}^{0.298}$ $(r^2 = 0.55, N = 55)$ (hereafter denoted R01). When extrapolated to other wavelengths using the spectral slope they got from their data set ($S = 0.0195$ nm^{-1}), it agrees quite well with our relationships (Fig. 6d,e,f).

3.4 $a_y(\lambda)$ distribution

Histograms of retrieved $a_y(\lambda)$ and corresponding spectral slopes are shown in Fig. 7. The mode values of a_y in the SO are 0.021 m^{-1} at 380 nm, 0.0161 m^{-1} at 412 nm, and 0.0084 m^{-1} at 490 nm. For the low-latitude waters, the corresponding values are 0.015, 0.0082 and approximately zero. Notably, 24% of the $a_y(490)$ retrievals are negative, compared with 2% at 380 nm and 5% at 412 nm. In the low-latitude waters, the respective percentages are 41%, 5% and 12%. This is expected, as $a_y(490)$ is significantly smaller than $a_y(380)$ (due to the exponential decrease with wavelength) and because the method has larger uncertainty at 490 nm. Additionally, the spectral slope of $a_y(\lambda)$, S (nm^{-1}), was calculated as the average of the a_y spectral dependence between 380 and 490 nm and between 412 and 490 nm. The median value of S in the SO is 0.01 nm^{-1} and 0.013 nm^{-1} for the low-latitude waters. The latter is close to the value of 0.014 m^{-1} reported by Bricaud et al., (1981).

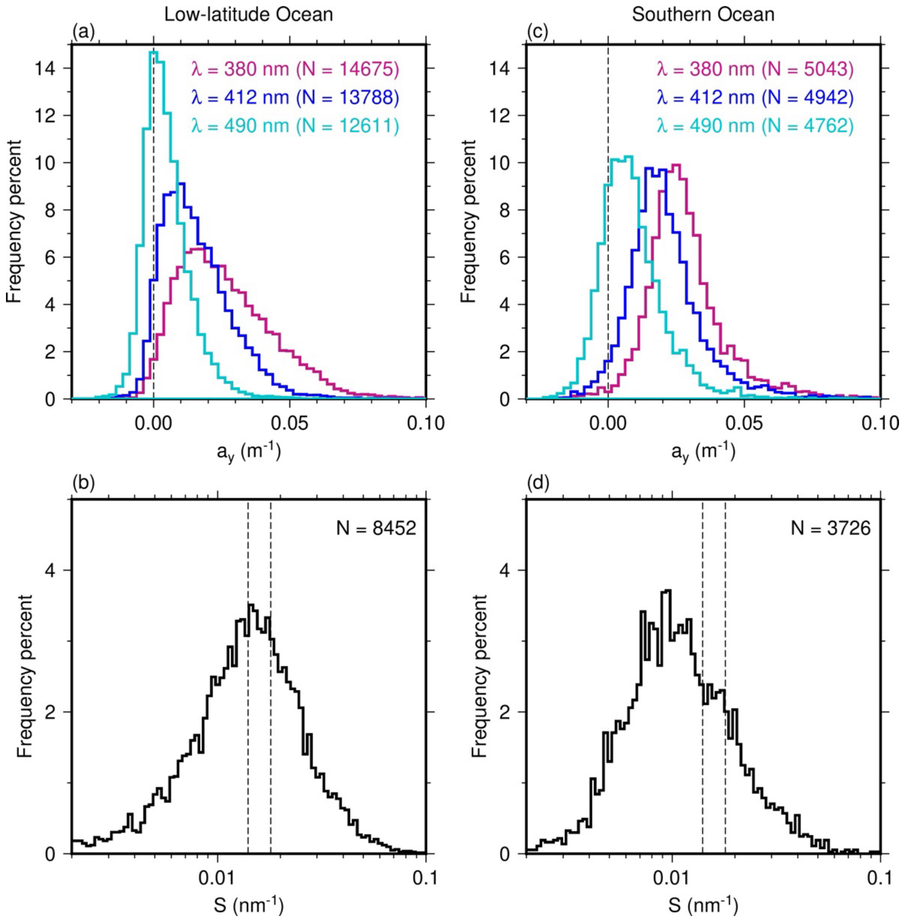

Figure 7: Distributions of a_y at the three wavelengths indicated and for the low-latitude Ocean (left) and the SO (right). The corresponding spectral slopes are displayed in (c) and (d). The dashed lines in (c) and (d) are the S values proposed by Bricaud et al., (1981) (0.014 nm^{-1}) and those used by Morel and Gentili (2009) (0.018 nm^{-1}).

https://doi.org/10.5194/egusphere-2025-5495
Preprint. Discussion started: 24 November 2025

The latitudinal distributions of the average $a_y(380)$ and Chl, calculated from all data available in 2-degree latitude belts, are illustrated in Fig. 8. Generally, $a_y(380)$ fluctuates between about 0.01 and 0.04 m^{-1} south of 30° S, which is larger than the range observed in low-latitude waters (30° S – 30° N), where values around 0.01 m^{-1} are quite frequent. This is consistent with larger DOC concentrations previously reported in the SO (e.g., Lechtenfeld et al., 2014). Larger values are observed north of 30° N with the increase of Chl towards northern latitudes. This distribution varies little seasonally (not shown).

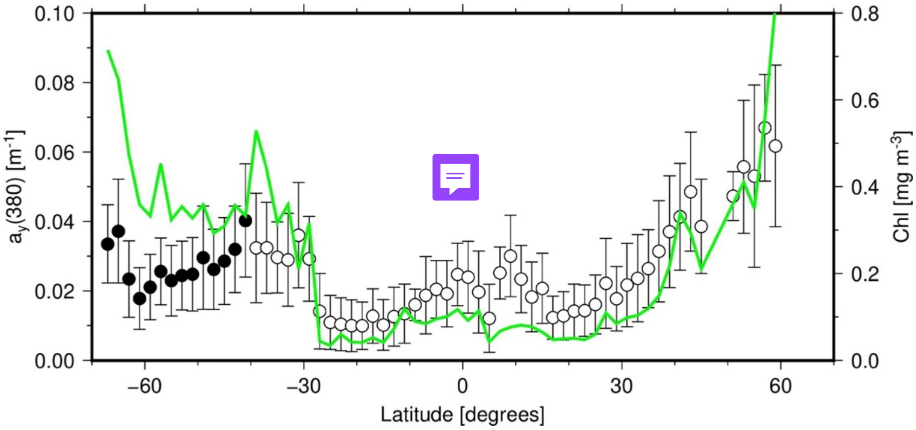

Figure 8: Zonal averages and standard deviation of $a_y(380)$ for 2-degree latitude bands, calculated across our entire data set. The green curve is for Chl (no standard deviation plotted for clarity of the plot). Black dots are for latitudes south of 40° S.

When the same data are used to assess the general relationship between $a_y(380)$ and Chl, they show a clear correlation (Fig. 9) and generally they align with the MG09 relationship, except for the SO data, which display lower $a_y(380)$ values than most of the low-latitude data for Chl > ~0.2 mg m^{-3}. This is consistent with what is shown in Fig. 6.

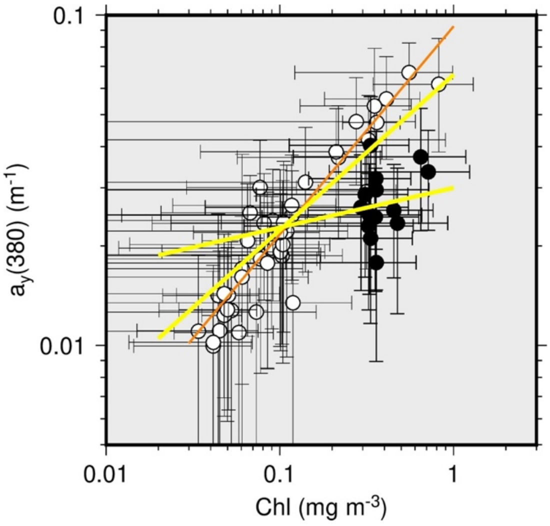

Figure 9: Scatter plot of $a_y(380)$ vs. Chl, from the data shown in Fig. 8 (error bars are the standard deviations). Black dots are for latitudes south of 40° S. The orange line is the Morel and Gentili (2009) relationship and the two yellow lines are the relationships displayed in Fig. 6a and 6d.

4 Discussion

4.1 Uncertainties of a_y estimates

There are several sources of uncertainty when deriving a_y from K_d using Eq. (4) without concomitant measurements of the various parameters of the equation. These uncertainties were assessed and shown non negligible. Nevertheless, meaningful a_y vs. Chl relationships could be derived thanks to the large number of points in our data sets. Our uncertainty assessment did not consider possible systematic large biases in the initial K_d values. The results in Fig. 5, including the comparison with MM01, did not show evidence that such biases are present.

The adjustment we applied to the Chl values for the low-latitude areas is another source of uncertainty. When it is not performed, the slope of the a_y vs. Chl changes slightly (e.g., from 0.57 to 0.45 at $\lambda = 412$ nm), yet the observation that a_y in the SO does not vary with Chl as strongly as it does in the low-latitude areas still holds.

4.2 Possible reasons for the weak dependence of a_y on Chl in the SO

CDOM in open waters derives from local sources, through *in situ* production in the euphotic zone and redistribution via horizontal and vertical circulation. The latter is mainly driven by physical processes such as winter seasonal mixing, upwelling and storms that bring CDOM to the surface ocean (Nelson and Siegel, 2013; Mannino et al., 2014). While the former is related to a wide range of biological processes including viral lysis, bacterial degradation, phytoplankton excretion and zooplankton grazing (Bricaud et al., 1981; Nelson et al., 1998; Nelson and Siegel, 2002; Siegel et al., 2002; Matsuoka et al., 2013; Bonelli et al., 2021). Loss mechanisms also determine the CDOM balance, including microbial consumption and photooxidation (Siegel et al., 2002; Nelson et al., 2007). Consequently, the dynamics of CDOM are strongly regulated by the interplay between physical and biogeochemical processes.

Our results show that this interplay of multiple physical and biological processes in the SO leads to different CDOM dynamics as compared to lower latitude waters. The SO is structured by a succession of oceanic fronts that tend to isolate water masses (Park et al., 2019), experiences seasonal sea ice melt that releases organic matter in surface waters (Norman et al., 2011; Ortega-Retuerta et al., 2010), and is home of pronounced vertical mixing (Olbers and Visbeck, 2005; Hillenbrand and Cortese, 2006). These characteristics create highly heterogeneous environments that influence the sources, transformations, and distribution of CDOM. In addition, the phytoplankton communities in the SO exhibit distinct physiological adaptations to the extreme light-limited conditions, which likely alter their production and release of CDOM compared to those in more illuminated waters (Strzepek et al., 2019). Collectively, these factors introduce substantial variability into a_y dynamics and apparently weaken its direct coupling with Chl, making Chl a poor predictor of a_y in these high-latitude waters.

4.3 Do Southern Ocean waters belong to Case 1 waters?

The concept of Case 1 vs. Case 2 waters (Morel and Prieur, 1977) has been instrumental by providing a global and consistent framework to quantitatively interpret satellite ocean color observations. The concept is based on the observation that biological matter that drives bio-optical properties and hence ocean color covaries with phytoplankton in open ocean waters, classified as Case 1 waters. Therefore, Chl can be used as a single index of changes in ocean color in such waters, which does not mean that it is the sole responsible for changes. Assuming this co-variability when deriving empirical chlorophyll algorithms, for instance, does not require separate consideration of how the components of the biological matter individually correlate with Chl (e.g., phytoplankton, detrital matter, CDOM). Variability in these relationships are a large source of uncertainty in the Chl retrieval from satellite ocean color and have led to questioning whether the concept itself was useful (Mobley et al., 2004). When semi-analytical algorithms are developed, however, phytoplankton, non-algal particles and dissolved substances each have their own relationship to Chl (e.g., Bricaud et al., 1998; Maritorena et al., 2002; Morel and Gentili, 2009). Improved retrievals of Chl from satellite ocean color observations over the SO will require revision of how CDOM absorption is parameterized.

Authors contributions

Juan Li: Conceptualization (equal), data curation (equal), formal analysis (equal), investigation (equal), methodology (equal), software (equal), visualization (equal), writing– original draft (lead), writing– review & editing (equal). **David Antoine**: Conceptualization (equal), data curation (equal), formal analysis (equal), methodology (equal), software (equal), visualization (equal), funding acquisition (lead), resources (lead), supervision (lead), writing– original draft (lead), writing– review & editing (equal). **Yannick Huot**: Conceptualization (equal), supervision (supporting), writing– review & editing (supporting).

Data availability statement

Publicly available datasets were analyzed in this study. They can be found here: BGC-Argo float data is available at https://biogeochemical-argo.org. Data collected during cruises are available at https://zenodo.org/records/3993096, https://doi.org/10.5281/zenodo.3816726, https://doi.org/10.5281/zenodo.3660852, https://doi.org/10.5281/zenodo.3706710. The processing code, figure scripts and information on data sets are available at: https://github.com/dvantoine/CDOMpaper2025.

Funding

Juan Li was supported by the Australian Research Council Special Research Initiative, Australian Centre for Excellence in Antarctic Science (ACEAS; Project Number SR200100008). ACE was funded by Ferring Pharmaceuticals with additional support from the Swiss Polar Institute. Funding from the Australian Research Council Discovery Program (DP160103387) contributed to the exploitation of the ACE data.

Conflict of interest

The authors declare that the research was conducted in the absence of any commercial or financial relationships that could be construed as a potential conflict of interest.

References

Antoine, D., Chami, M., Claustre, H., Gentili, B., Louis, F., Ras, J., Roussier, E., Scott, A. J., Tailliez, D., Hooker, S. B., Guevel, P., Desté, J.-F., Dempsey, C., and Adams, D.: BOUSSOLE: A Joint CNRS-INSU, ESA, CNES, and NASA Ocean Color

Calibration and Validation Activity, 2006.

Antoine, D., Thomalla, S., Berliner, D., Little, H., Moutier, W., Olivier-Morgan, A., Robinson, C., Ryan-Keogh, T., and Schuback, N.: Particulate light absorption coefficients (350 – 750 nm) measured using the filter pad method during the Antarctic Circumnavigation Expedition (ACE) during the austral summer of 2016/2017. (1.0), https://doi.org/10.5281/zenodo.3993096, 2021.

Argo data management: Argo user's manual, 2025. https://doi.org/10.13155/29825

Aurin, D., Mannino, A., and Lary, D. J.: Remote Sensing of CDOM, CDOM Spectral Slope, and Dissolved Organic Carbon in the Global Ocean, Applied Sciences, 8, 2687, https://doi.org/10.3390/app8122687, 2018.

Bonelli, A. G., Vantrepotte, V., Jorge, D. S. F., Demaria, J., Jamet, C., Dessailly, D., Mangin, A., Fanton d'Andon, O., Kwiatkowska, E., and Loisel, H.: Colored dissolved organic matter absorption at global scale from ocean color radiometry observation: Spatio-temporal variability and contribution to the absorption budget, Remote Sensing of Environment, 265, 112637, https://doi.org/10.1016/j.rse.2021.112637, 2021.

Boyd, P. W., Arrigo, K. R., Ardyna, M., Halfter, S., Huckstadt, L., Kuhn, A. M., Lannuzel, D., Neukermans, G., Novaglio, C., Shadwick, E. H., Swart, S., and Thomalla, S. J.: The role of biota in the Southern Ocean carbon cycle, Nat Rev Earth Environ, 5, 390–408, https://doi.org/10.1038/s43017-024-00531-3, 2024.

Bricaud, A., Morel, A., and Prieur, L.: Absorption by dissolved organic matter of the sea (yellow substance) in the UV and visible domains1, Limnol. Oceanogr., 26, 43–53, https://doi.org/10.4319/lo.1981.26.1.0043, 1981.

Bricaud, A., Morel, A., Babin, M., Allali, K., and Claustre, H.: Variations of light absorption by suspended particles with chlorophyll a concentration in oceanic (case 1) waters: Analysis and implications for bio-optical models, Journal of Geophysical Research: Oceans, 103, 31033–31044, https://doi.org/10.1029/98JC02712, 1998.

Bricaud, A., Babin, M., Claustre, H., Ras, J., and Tièche, F.: Light absorption properties and absorption budget of Southeast Pacific waters, J. Geophys. Res., 115, C08009, https://doi.org/10.1029/2009JC005517, 2010.

Cao, F. and Miller, W. L.: A new algorithm to retrieve chromophoric dissolved organic matter (CDOM) absorption spectra in the UV from ocean color, Journal of Geophysical Research: Oceans, 120, 496–516, https://doi.org/10.1002/2014JC010241, 2015.

Cao, F., Tzortziou, M., Hu, C., Mannino, A., Fichot, C. G., Del Vecchio, R., Najjar, R. G., and Novak, M.: Remote sensing retrievals of colored dissolved organic matter and dissolved organic carbon dynamics in North American estuaries and their margins, Remote Sensing of Environment, 205, 151–165, https://doi.org/10.1016/j.rse.2017.11.014, 2018.

Carder, K. L., Chen, F., Lee, Z., Hawes, S., and Kamykowski, D.: Semianalytic Moderate-Resolution Imaging Spectrometer algorithms for chlorophyll a and absorption with bio-optical domains based on nitrate-depletion temperatures, Journal of Geophysical Research: Oceans, 104, 5403–5421, 1999.

Chen, J., Zhu, W., Tian, Y. Q., Yu, Q., Zheng, Y., and Huang, L.: Remote estimation of colored dissolved organic matter and chlorophyll-a in Lake Huron using Sentinel-2 measurements, JARS, 11, 036007, https://doi.org/10.1117/1.JRS.11.036007, 2017.

Claustre, H., Sciandra, A., and Vaulot, D.: Introduction to the special section bio-optical and biogeochemical conditions in the South East Pacific in late 2004: the BIOSOPE program, Biogeosciences, 5, 679–691, 2008.

Claustre, H., Johnson, K. S., and Takeshita, Y.: Observing the Global Ocean with Biogeochemical-Argo, Annual Review of Marine Science, 12, 23–48, https://doi.org/10.1146/annurev-marine-010419-010956, 2020.

Dall'Olmo, G., Westberry, T. K., Behrenfeld, M. J., Boss, E., and Slade, W. H.: Significant contribution of large particles to optical backscattering in the open ocean, Biogeosciences, 6, 947–967, https://doi.org/10.5194/bg-6-947-2009, 2009.

Gordon, H. R.: Dependence of the diffuse reflectance of natural waters on the sun angle: Diffuse reflectance dependence on sun angle, Limnol. Oceanogr., 34, 1484–1489, https://doi.org/10.4319/lo.1989.34.8.1484, 1989.

https://doi.org/10.5194/egusphere-2025-5495
Preprint. Discussion started: 24 November 2025

Gregg, W. W. and Carder, K. L.: A simple spectral solar irradiance model for cloudless maritime atmospheres, Limnology and Oceanography, 35, 1657–1675, https://doi.org/10.4319/lo.1990.35.8.1657, 1990.

Gruber, N., Gloor, M., Mikaloff Fletcher, S. E., Doney, S. C., Dutkiewicz, S., Follows, M. J., Gerber, M., Jacobson, A. R., Joos, F., Lindsay, K., Menemenlis, D., Mouchet, A., Müller, S. A., Sarmiento, J. L., and Takahashi, T.: Oceanic sources, sinks, and transport of atmospheric CO2, Global Biogeochemical Cycles, 23, 1–21, https://doi.org/10.1029/2008GB003349, 2009.

Gruber, N., Landschützer, P., and Lovenduski, N. S.: The Variable Southern Ocean Carbon Sink, Annual Review of Marine Science, 11, 159–186, https://doi.org/10.1146/annurev-marine-121916-063407, 2019.

Hauck, J., Gregor, L., Nissen, C., Patara, L., Hague, M., Mongwe, P., Bushinsky, S., Doney, S. C., Gruber, N., Le Quéré, C., Manizza, M., Mazloff, M., Monteiro, P. M. S., and Terhaar, J.: The Southern Ocean Carbon Cycle 1985–2018: Mean, Seasonal Cycle, Trends, and Storage, Global Biogeochemical Cycles, 37, e2023GB007848, https://doi.org/10.1029/2023GB007848, 2023.

Hillenbrand, C.-D. and Cortese, G.: Polar stratification: A critical view from the Southern Ocean, Palaeogeography, Palaeoclimatology, Palaeoecology, 242, 240–252, https://doi.org/10.1016/j.palaeo.2006.06.001, 2006.

Hooker, S. B. and Zibordi, G.: Advanced Methods for Characterizing the Immersion Factor of Irradiance Sensors, J. Atmos. Oceanic Technol., 22, 757–770, https://doi.org/10.1175/JTECH1736.1, 2005.

Houskeeper, H. F., Hooker, S. B., and Kudela, R. M.: Spectral range within global aCDOM(440) algorithms for oceanic, coastal, and inland waters with application to airborne measurements, Remote Sensing of Environment, 253, 112155, https://doi.org/10.1016/j.rse.2020.112155, 2021.

Jamet, C., Loisel, H., and Dessailly, D.: Retrieval of the spectral diffuse attenuation coefficient Kd(λ) in open and coastal ocean waters using a neural network inversion, Journal of Geophysical Research: Oceans, 117, https://doi.org/10.1029/2012JC008076, 2012.

Lechtenfeld, O. J., Kattner, G., Flerus, R., McCallister, S. L., Schmitt-Kopplin, P., and Koch, B. P.: Molecular transformation and degradation of refractory dissolved organic matter in the Atlantic and Southern Ocean, Geochimica et Cosmochimica Acta, 126, 321–337, https://doi.org/10.1016/j.gca.2013.11.009, 2014.

Lee, Z., Carder, K. L., and Arnone, R. A.: Deriving inherent optical properties from water color: a multiband quasi-analytical algorithm for optically deep waters, Appl. Opt., 41, 5755, https://doi.org/10.1364/AO.41.005755, 2002.

Lee, Z., Wei, J., Voss, K., Lewis, M., Bricaud, A., and Huot, Y.: Hyperspectral absorption coefficient of “pure” seawater in the range of 350–550 nm inverted from remote sensing reflectance, Appl. Opt., 54, 546, https://doi.org/10.1364/AO.54.000546, 2015.

Li, J., Antoine, D., and Huot, Y.: Bio-optical variability of particulate matter in the Southern Ocean, Frontiers in Marine Science, https://doi.org/10.3389/fmars.2024.1466037, 2024.

Loisel, H., Mangin, A., Vantrepotte, V., Dessailly, D., Ngoc Dinh, D., Garnesson, P., Ouillon, S., Lefebvre, J.-P., Mériaux, X., and Minh Phan, T.: Variability of suspended particulate matter concentration in coastal waters under the Mekong’s influence from ocean color (MERIS) remote sensing over the last decade, Remote Sensing of Environment, 150, 218–230, https://doi.org/10.1016/j.rse.2014.05.006, 2014.

Mannino, A., Russ, M. E., and Hooker, S. B.: Algorithm development and validation for satellite-derived distributions of DOC and CDOM in the U.S. Middle Atlantic Bight, Journal of Geophysical Research: Oceans, 113, https://doi.org/10.1029/2007JC004493, 2008.

Mannino, A., Novak, M. G., Hooker, S. B., Hyde, K., and Aurin, D.: Algorithm development and validation of CDOM properties for estuarine and continental shelf waters along the northeastern U.S. coast, Remote Sensing of Environment, 152, 576–602, https://doi.org/10.1016/j.rse.2014.06.027, 2014.

Maritorena, S., Siegel, D. A., and Peterson, A. R.: Optimization of a semianalytical ocean color model for global-scale applications, Appl. Opt., 41, 2705, https://doi.org/10.1364/AO.41.002705, 2002.

Matsuoka, A., Hooker, S. B., Bricaud, A., Gentili, B., and Babin, M.: Estimating absorption coefficients of colored dissolved organic matter (CDOM) using a semi-analytical algorithm for southern Beaufort Sea waters: application to deriving concentrations of dissolved organic carbon from space, Biogeosciences, 10, 917–927, https://doi.org/10.5194/bg-10-917-2013, 2013.

Mobley, C. D., Stramski, D., Paul Bissett, W., and Boss, E.: Optical modeling of ocean waters: Is the case 1 - case 2 classification still useful?, Oceanography, 17, 60, https://doi.org/10.5670/oceanog.2004.48, 2004.

Moore, T. S., Campbell, J. W., and Dowell, M. D.: A class-based approach to characterizing and mapping the uncertainty of the MODIS ocean chlorophyll product, Remote Sensing of Environment, 113, 2424–2430, https://doi.org/10.1016/j.rse.2009.07.016, 2009.

Morel, A.: Optical modeling of the upper ocean in relation to its biogenous matter content (case I waters), J. Geophys. Res., 93, 10749, https://doi.org/10.1029/JC093iC09p10749, 1988.

Morel, A. and Gentili, B.: Radiation transport within oceanic (case 1) water, Journal of Geophysical Research: Oceans, 109, https://doi.org/10.1029/2003JC002259, 2004.

Morel, A. and Gentili, B.: A simple band ratio technique to quantify the colored dissolved and detrital organic material from ocean color remotely sensed data, Remote Sensing of Environment, 113, 998–1011, https://doi.org/10.1016/j.rse.2009.01.008, 2009.

Morel, A. and Maritorena, S.: Bio-optical properties of oceanic waters: A reappraisal, J. Geophys. Res., 106, 7163–7180, https://doi.org/10.1029/2000JC000319, 2001.

Morel, A. and Prieur, L.: Analysis of variations in ocean color1: Ocean color analysis, Limnol. Oceanogr., 22, 709–722, https://doi.org/10.4319/lo.1977.22.4.0709, 1977.

Morel, A., Antoine, D., and Gentili, B.: Bidirectional reflectance of oceanic waters: accounting for Raman emission and varying particle scattering phase function, Appl. Opt., 41, 6289, https://doi.org/10.1364/AO.41.006289, 2002.

Morel, A., Claustre, H., Antoine, D., and Gentili, B.: Natural variability of bio-optical properties in Case 1 waters: attenuation and reflectance within the visible and near-UV spectral domains, as observed in South Pacific and Mediterranean waters, mg m, 2007a.

Morel, A., Gentili, B., Claustre, H., Babin, M., Bricaud, A., Ras, J., and Tièche, F.: Optical properties of the “clearest” natural waters, Limnol. Oceanogr., 52, 217–229, https://doi.org/10.4319/lo.2007.52.1.0217, 2007b.

Nelson, N. B. and Siegel, D. A.: Chromophoric DOM in the open ocean, Biogeochemistry of marine dissolved organic matter, 547–578, 2002.

Nelson, N. B. and Siegel, D. A.: The Global Distribution and Dynamics of Chromophoric Dissolved Organic Matter, Annual Review of Marine Science, 5, 447–476, https://doi.org/10.1146/annurev-marine-120710-100751, 2013.

Nelson, N. B., Siegel, D. A., and Michaels, A. F.: Seasonal dynamics of colored dissolved material in the Sargasso Sea, Deep Sea Research Part I: Oceanographic Research Papers, 45, 931--957, 1998.

Nelson, N. B., Siegel, D. A., Carlson, Craig. A., Swan, C., Smethie, W. M., and Khatiwala, S.: Hydrography of chromophoric dissolved organic matter in the North Atlantic, Deep Sea Research Part I: Oceanographic Research Papers, 54, 710–731, https://doi.org/10.1016/j.dsr.2007.02.006, 2007.

NOAA National Geophysical Data Center: ETOPO1 1 Arc-Minute Global Relief Model, 2009.

Norman, L., Thomas, D. N., Stedmon, C. A., Granskog, M. A., Papadimitriou, S., Krapp, R. H., Meiners, K. M., Lannuzel, D., van der Merwe, P., and Dieckmann, G. S.: The characteristics of dissolved organic matter (DOM) and chromophoric dissolved organic matter (CDOM) in Antarctic sea ice, Deep Sea Research Part II: Topical Studies in Oceanography, 58, 1075–1091, https://doi.org/10.1016/j.dsr2.2010.10.030, 2011.

Olbers, D. and Visbeck, M.: A Model of the Zonally Averaged Stratification and Overturning in the Southern Ocean, Journal of

Physical Oceanography, 35, 1190–1205, https://doi.org/10.1175/JPO2750.1, 2005.

Organelli, E., Bricaud, A., Antoine, D., and Matsuoka, A.: Seasonal dynamics of light absorption by chromophoric dissolved organic matter (CDOM) in the NW Mediterranean Sea (BOUSSOLE site), Deep Sea Research Part I: Oceanographic Research Papers, 91, 72–85, https://doi.org/10.1016/j.dsr.2014.05.003, 2014.

Organelli, E., Claustre, H., Bricaud, A., Schmechtig, C., Poteau, A., Xing, X., Prieur, L., D'Ortenzio, F., Dall'Olmo, G., and Vellucci, V.: A Novel Near-Real-Time Quality-Control Procedure for Radiometric Profiles Measured by Bio-Argo Floats: Protocols and Performances, Journal of Atmospheric and Oceanic Technology, 33, 937–951, https://doi.org/10.1175/JTECH-D-15-0193.1, 2016.

Ortega-Retuerta, E., Reche, I., Pulido-Villena, E., Agustí, S., and Duarte, C. M.: Distribution and photoreactivity of chromophoric dissolved organic matter in the Antarctic Peninsula (Southern Ocean), Marine Chemistry, 118, 129–139, https://doi.org/10.1016/j.marchem.2009.11.008, 2010.

Park, Y.-H., Park, T., Kim, T.-W., Lee, S.-H., Hong, C.-S., Lee, J.-H., Rio, M.-H., Pujol, M.-I., Ballarotta, M., Durand, I., and Provost, C.: Observations of the Antarctic Circumpolar Current Over the Udintsev Fracture Zone, the Narrowest Choke Point in the Southern Ocean, Journal of Geophysical Research: Oceans, 124, 4511–4528, https://doi.org/10.1029/2019JC015024, 2019.

Ras, J., Claustre, H., and Uitz, J.: Spatial variability of phytoplankton pigment distributions in the Subtropical South Pacific Ocean: comparison between in situ and predicted data, Biogeosciences, 5, 353–369, https://doi.org/10.5194/bg-5-353-2008, 2008.

Reynolds, R. A., Stramski, D., and Mitchell, B. G.: A chlorophyll-dependent semianalytical reflectance model derived from field measurements of absorption and backscattering coefficients within the Southern Ocean, Journal of Geophysical Research: Oceans, 106, 7125–7138, https://doi.org/10.1029/1999JC000311, 2001.

Reynolds, R. A., Stramski, D., and Neukermans, G.: Optical backscattering by particles in Arctic seawater and relationships to particle mass concentration, size distribution, and bulk composition: Particle backscattering in Arctic seawater, Limnol. Oceanogr., 61, 1869–1890, https://doi.org/10.1002/lno.10341, 2016.

Robinson, C. M., Huot, Y., Schuback, N., Ryan-Keogh, T. J., Thomalla, S. J., and Antoine, D.: High latitude Southern Ocean phytoplankton have distinctive bio-optical properties, Opt. Express, OE, 29, 21084–21112, https://doi.org/10.1364/OE.426737, 2021.

Roesler, C., Uitz, J., Claustre, H., Boss, E., Xing, X., Organelli, E., Briggs, N., Bricaud, A., Schmechtig, C., Poteau, A., D'Ortenzio, F., Ras, J., Drapeau, S., Haëntjens, N., and Barbieux, M.: Recommendations for obtaining unbiased chlorophyll estimates from in situ chlorophyll fluorometers: A global analysis of WET Labs ECO sensors, Limnology and Oceanography: Methods, 15, 572–585, https://doi.org/10.1002/lom3.10185, 2017.

Sarmiento, J. L., Johnson, K. S., Arteaga, L. A., Bushinsky, S. M., Cullen, H. M., Gray, A. R., Hotinski, R. M., Maurer, T. L., Mazloff, M. R., Riser, S. C., Russell, J. L., Schofield, O. M., and Talley, L. D.: The Southern Ocean carbon and climate observations and modeling (SOCCOM) project: A review, Progress in Oceanography, 219, 103130, https://doi.org/10.1016/j.pocean.2023.103130, 2023.

Siegel, D. A., Maritorena, S., Nelson, N. B., Hansell, D. A., and Lorenzi-Kayser, M.: Global distribution and dynamics of colored dissolved and detrital organic materials, Journal of Geophysical Research: Oceans, 107, 21-1-21–14, https://doi.org/10.1029/2001JC000965, 2002.

Strzepek, R. F., Boyd, P. W., and Sunda, W. G.: Photosynthetic adaptation to low iron, light, and temperature in Southern Ocean phytoplankton, Proceedings of the National Academy of Sciences, 116, 4388–4393, https://doi.org/10.1073/pnas.1810886116, 2019.

Werdell, P. J. and Bailey, S. W.: An improved in-situ bio-optical data set for ocean color algorithm development and satellite data product validation, Remote sensing of environment, 98, 122–140, https://doi.org/doi:10.1016/j.rse.2005.07.001, 2005.

Zhang, X. and Hu, L.: Estimating scattering of pure water from density fluctuation of the refractive index, Opt. Express, OE, 17, 1671–1678, https://doi.org/10.1364/OE.17.001671, 2009.

Zhang, X., Hu, L., and He, M.-X.: Scattering by pure seawater: Effect of salinity, Opt. Express, OE, 17, 5698–5710, https://doi.org/10.1364/OE.17.005698, 2009.

Zhu, W. and Yu, Q.: Inversion of Chromophoric Dissolved Organic Matter From EO-1 Hyperion Imagery for Turbid Estuarine and Coastal Waters, IEEE Transactions on Geoscience and Remote Sensing, 51, 3286–3298, https://doi.org/10.1109/TGRS.2012.2224117, 2013.

Zhu, W., Yu, Q., Tian, Y. Q., Chen, R. F., and Gardner, G. B.: Estimation of chromophoric dissolved organic matter in the Mississippi and Atchafalaya river plume regions using above-surface hyperspectral remote sensing, Journal of Geophysical Research: Oceans, 116, https://doi.org/10.1029/2010JC006523, 2011.

Zhu, W., Yu, Q., Tian, Y. Q., Becker, B. L., Zheng, T., and Carrick, H. J.: An assessment of remote sensing algorithms for colored dissolved organic matter in complex freshwater environments, Remote Sensing of Environment, 140, 766–778, https://doi.org/10.1016/j.rse.2013.10.015, 2014.